LUND UNIVERSITY

Atomistic investigation of functionalized polyethylene-alumina interfacial strength and tensile behaviour

Olsson, Pär; Bergvall, Erik

Published in:
Computational Materials Science

DOI:
10.1016/j.commatsci.2020.110075

2021

Document Version:
Publisher's PDF, also known as Version of record

Link to publication

Citation for published version (APA):
Olsson, P., & Bergvall, E. (2021). Atomistic investigation of functionalized polyethylene-alumina interfacial strength and tensile behaviour. *Computational Materials Science*, *187*, Article 110075. https://doi.org/10.1016/j.commatsci.2020.110075

Total number of authors:
2

Creative Commons License:
CC BY

General rights
Unless other specific re-use rights are stated the following general rights apply:
Copyright and moral rights for the publications made accessible in the public portal are retained by the authors and/or other copyright owners and it is a condition of accessing publications that users recognise and abide by the legal requirements associated with these rights.
• Users may download and print one copy of any publication from the public portal for the purpose of private study or research.
• You may not further distribute the material or use it for any profit-making activity or commercial gain
• You may freely distribute the URL identifying the publication in the public portal

Read more about Creative commons licenses: https://creativecommons.org/licenses/

Take down policy
If you believe that this document breaches copyright please contact us providing details, and we will remove access to the work immediately and investigate your claim.

LUND UNIVERSITY

PO Box 117
221 00 Lund
+46 46-222 00 00

Computational Materials Science 187 (2021) 110075

Contents lists available at ScienceDirect

Computational Materials Science

journal homepage: www.elsevier.com/locate/commatsci

Atomistic investigation of functionalized polyethylene-alumina interfacial strength and tensile behaviour

Pär A.T. Olsson [a,b,*], Erik Bergvall [c]

[a] Materials Science and Applied Mathematics, Malmö University, SE-205 06 Malmö, Sweden
[b] Division of Mechanics, Lund University, Box 118, SE-221 00 Lund, Sweden
[c] Tetra Pak Packaging Solutions AB, Ruben Rausings gata, SE-221 86 Lund, Sweden

ARTICLE INFO

Keywords:
Adhesion
Polyethylene
Alumina
Molecular dynamics
Density functional theory

ABSTRACT

We study the adhesion and tensile behaviour of bi-layer interfaces comprising polyethylene, doped with carbonyl and hydroxyl functional groups emanating from ozone treatment, and α-Al_2O_3 by means of density functional theory and classical atomistic modelling. The results show that the deformations are localized within the polymer and comprise chain slip, disentanglement and detachment from the substrate, where only the latter is notably affected by the doping. The binding energies and excess forces associated with the detachment of functional groups from the alumina substrate are of the order of 1.7 eV and 1 nN, respectively, for both types. Although such forces do not affect the maximum peak stress notably, they give rise to spikes in the traction-separation curves following the fibril formation and promote increased total work of fracture.

1. Introduction

To limit the degradation and prolong the shelf-life, today's food and beverage containers are typically engineered and highly optimized to guarantee that the content exposure to environmental and other contaminants are kept to a minimum. This includes for instance direct sunlight and/or air exposure, that individually or jointly can contribute to photodegradation of the content [1], which can lead to e.g. oxidation of fats and oils, the formation of unpleasant off-flavors, losses of various vitamins etc. [2,3]. Thus, designing food containers requires optimization such that it can maintain the structural integrity throughout the life-cycle - which may include wet and cold storage conditions and heating and large deformations during production - while simultaneously meeting demands for reduced material expenditures to limit the environmental footprint.

For containers with products that are sensitive to light, the walls are typically multi-layered composite laminate structures that contain barriers consisting of thin layered polyethylene (PE) sheets adhered onto aluminium foils [4]. To join them, the use of adhesives between layers must be limited to products that are non–hazardous to health. Thus, it is common to utilize means that rely on surface treatments to enhance the bonding between layers. For instance plasma treatments are used to alter the surface properties to improve the conditions for adhesion [5]. Such techniques can be used for the creation of polar groups to enchance the adhesion and/or to remove unwanted organic surface contaminations, e.g. rolling oil residues, that can reduce the interfacial attraction. Plasma treatments do not only provide surface modification during the plasma exposure, but also typically leave active sites that are available for post-reactions, commonly referred to as aging, which through e.g. diffusion processes can lead to surface restructuring and further enhanced adhesion. Moreover, ozone treatment of the PE melt and aluminium foil is a commonly used technique that aims to increase the coverage of hydroxyl and carbonyl groups on the surfaces [6], which can act as Lewis acid and base pairs and greatly strengthen the adhesion between the layers [7,8].

Predicting the adhesive strength of functionalized interfaces is a multi-disciplinary problem that ultimately depends on the surface character and the atomic interaction across the interface. Even though atomistic modelling is a useful modelling tool to gain insight on the matter, such techniques have been sparsely utilized to investigate the mechanics of aluminium/alumina-PE interfaces, despite its importance. Most works have involved *ab initio* density functional theory (DFT) modelling of adhesion of individual functional groups, e.g. various alcohol molecules [9,10], epoxy resins [11], methylamine [12], polycarbonate functional groups [13,14], onto aluminium or alumina surfaces. Such electronic scale modelling provides valuable insight on the

* Corresponding author at: Materials Science and Applied Mathematics, Malmö University, SE-205 06 Malmö, Sweden.
E-mail address: Par.Olsson@mau.se (P.A.T. Olsson).

https://doi.org/10.1016/j.commatsci.2020.110075
Received 1 September 2020; Received in revised form 21 September 2020; Accepted 22 September 2020
0927-0256/© 2020 The Author(s). Published by Elsevier B.V. This is an open access article under the CC BY license (http://creativecommons.org/licenses/by/4.0/).

electronic mechanisms behind the adhesion, preferential adsorption sites and can be used to quantify the bonding strength between the individual groups and the substrate.

The overwhelming computational cost associated with DFT modelling makes it impractical to model larger systems. For such problems, instead one has to rely on classical atomistic modelling, such as molecular dynamics (MD) or molecular statics (MS), in which the atoms interact through semi-empirical and predefined potentials. Although the interatomic interaction is simplified compared to electronic scale modelling, the number of particles that can be considered reaches well-beyond the capability of DFT, which enables the modelling of complex deformation mechanisms on a larger length scale than is presently attainable with DFT. In light of these benefits, classical techniques have been used to study single chain adsorption onto alumina surfaces for polymer chains containing functional groups [15]. The general outcome was that most functional groups increase the adsorption energy, while alkyl side groups attached to the backbone promote reduced adsorption energy. Classical atomistic modelling has also been successfully used for describing the deformation mechanisms and tensile strength of different types of interfaces, including e.g. ceramic-organic composites [16–18], metal-epoxy systems [19,20], binder-current collector interfaces [21], polymer-coated nano-particles [22] and metal-polymer interfaces in micro-injection moulding applications [23–25]. These works illustrate widely different deformation behaviours at composite interfaces as polymers with high glass temperatures, such as cross-linked epoxy and polyvinyl-alcohol (PVA), exhibit a more brittle and clean detachment from the substrate [16,19,20], whereas those with lower glass temperatures (e.g. polyvinylidene fluoride (PVDF) [21] and polypropylene [23]) undergo a higher degree of polymer deformation.

In light of these observations, PE-alumina interfaces are expected to deform in a ductile manner, as PE has a low glass temperature. However, since PE only interacts weakly with alumina, the interfacial strength is also expected to be low, which makes it unclear how the deformations will ensue - whether a clean separation or localized plastic deformations in the polymer will occur before fracture? It is also of interest to quantify the impact of ozone-induced functional groups on the fracture energy to gain insight on the extent to which they affect the response and deformation mechanisms. Such knowledge is necessary to explain the macroscopic behaviour of interfacial deformation and to optimize the design and production process for improved performance. To address these issues we use MD and MS modelling to study the deformation mechanisms and interfacial strength of α-Al_2O_3 and functionalized PE interfaces subjected to mode I tensile loading. The PE part of the interface is assumed to be amorphous, and to mimic ozone treatments we introduce randomly distributed hydroxyl or carbonyl groups in the polymer. To gain insight on the adhesion of individual functional groups and to ensure qualitative predictability of the adopted force-field, we resort to van der Waals (vdW) based DFT modelling to investigate and benchmark the binding energy of individual molecules onto alumina surfaces.

The paper is organised as follows: in the next section we describe the details of the setups and the atomistic modelling approaches, which are followed by a presentation and discussion of the results. Finally, the paper ends with a short summary of the work and a digest of the key findings.

2. Method

2.1. Interatomic interaction

For the classical atomistic modelling in this work, we use the open-source LAMMPS software [26]. For modelling polymers, the molecules can be represented either through all-atomic or coarse-grained approaches, where the beads are merged to form united-atoms. The benefit of the latter is that it enables longer time integration steps and leads to fewer degrees of freedom in the model. However, it was recently demonstrated in [27,28] that the united-atom approach fails to describe the generalized stacking fault behaviour of crystalline PE and gives rise to excessive chain slip. This limitation was attributed to the lack of explicit close-ranged H-H and C–H repulsion to describe the internal friction within the united-atom approach. Thus, for the modelling in the present work we used an all-atomic approach. Due to the explicit treatment of the light H-atoms in the model, to resolve the trajectories accurately, a relatively small time integration step size was required. Hence, for all simulations we used the integration timestep of 0.3 fs, which was found to be sufficiently small to conserve the mechanical energy in the NVE ensemble.

There is a number of different general-purpose interatomic potentials available for all-atomic modelling, including the COMPASS [29], the polymer consistent force-field (PCFF) [30,31] and the optimized potential for liquid simulations (OPLS-AA) [32,33]. In the present work we performed tensile modelling of pure PE using PCFF and OPLS-AA and found similar response and tensile behaviour for both potentials and therefore settled on using the PCFF potential as implemented in the MedeA software [34]. For describing the interaction of the alumina substrate we also adopted the PCFF but adjusted the atomic charges to those of Zhao et al. [35] to improve the electrostatic interaction with the organic elements. Within the assumed modelling framework, the assigned charges, q_i, remained unchanged throughout the simulations and such that no charge redistribution or change in bond order could occur. We also assumed that the partial charges associated with the elements in the substrate did not vary based on local coordination, instead fixed charges in line with those in [35] and substrate charge neutrality were adopted throughout the modelling.

The interaction between the alumina-substrate and the polymer comprises electrostatic and vdW dispersion interaction, which are described through Coulombic interaction and the Lennard-Jones 9-6 (LJ-9-6) potential, i.e.,

$$V(r_{ij}) = \frac{q_i q_j}{r_{ij}} + \varepsilon\left[2\left(\frac{\sigma}{r_{ij}}\right)^9 - 3\left(\frac{\sigma}{r_{ij}}\right)^6\right] \quad (1)$$

Most of the mixed parameters of the LJ-9–6 potential for the substrate and polymer were computed through the sixth power mixing rule [29]. However, to make sure that the adhesive strength of carbonyl and hydroxyl groups on alumina surfaces were accurately reproduced, we modelled the interaction between the alumina (0001)-surface and single molecules of acetaldehyde (CH_3CHO) and ethanol (C_2H_5OH) by means of DFT modelling and adjusted the mixed LJ-9–6 parameters (i.e. ε and σ of (1)) between substrate Al and molecular O to improve the bond strength agreement with the DFT results. The used parameters were obtained through systematic testing by varying the combination of ε and σ to approximately reproduce the effective potential well depth of the DFT data, while ensuring that the equilibrium bond length did not deviate more than ~0.5 Å. The cutoff for the real-space Coulombic interaction and LJ-9–6 potential was chosen to be 12 Å. The long-range Coulombic and r^{-6} interaction were computed using the PPPM summation method with a relative force accuracy of 10^{-6}.

2.2. Sample generation and geometry setup

The considered geometries are bi-layer composite structures that consist of an alumina substrate in contact with an amorphous polymer,

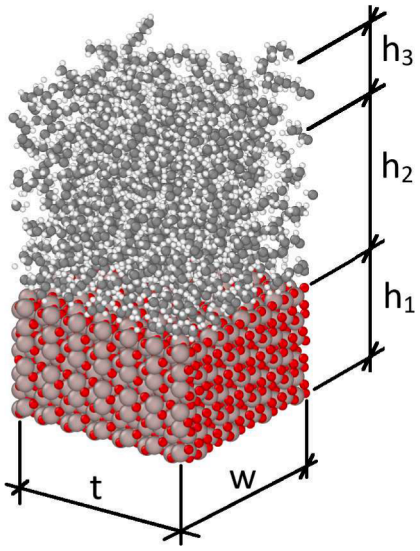

Fig. 1. Schematic of the alumina/polymer bi-layer structure. The large light grey and red particles represent Al and O, respectively, whereas the smaller dark grey and white particles are C and H atoms, respectively. The figure was generated using the OVITO software [36]. (For interpretation of the references to colour in this figure legend, the reader is referred to the web version of this article.)

see Fig. 1. The α-alumina phase has a hexagonal corundum structure and in the present work we represent the layer with a (0001)-surface, which is the most energetically favourable free surface for α-Al_2O_3 [37,38]. For all MD and MS modelling the substrate was assumed to be rigid with the geometry derived from relaxed DFT simulations of alumina (0001)-films using a vdW density functional (vdW-DF) approach (see below). Along the [0001]-direction, the corundum structure is layered with a R-Al-Al-O_3-R repetitive sequence, for which DFT and experimental works have predicted that it is preferential to cleave the crystal between the neighbouring Al-layers, such that it is terminated by a single Al-layer [37,39–41]. This surface termination was adopted herein, but it should be noted that the outermost Al atoms underwent inwards relaxation to the extent that the distance between the outermost O- and Al-layers was only of the order 0.1 Å as opposed to 0.8 Å in the bulk, which is in accordance with previous DFT works [42,13]. The height of the slab was chosen to be $h_1 \approx 18$ Å for the classical simulations.

The amorphous polymers were constructed using an elaborate multi-step initialization and equilibration scheme similar to that outlined in [16]. First, random and amorphous periodic 3D polymer samples with a density of about 50% of the target density ($\rho \approx 0.91$ g/cm^3) were generated using the Monte Carlo algorithm of the amorphous module in the MedeA software [34]. For the systems containing hydroxyl or carbonyl groups (henceforth referred to as PE(OH) and PE(O), respectively) we generated polymer chains such that five percent of the monomers were randomly exhanged to contain functionalized carbonyl or hydroxyl monomers. The cell was then subjected to gradual compression to 125% of the target density through ten isotropic compressive increments each lasting for 100 ps, while simultaneously thermally equilibrating the system at 900 K in the canonical ensemble by means of a Nosé-Hoover thermostat [43,44]. The simulation cell was then incrementally expanded to reach the target density. This was followed by a gradual cooling from 900 K to room temperature through the employment of NVT dynamics during 7.5 ns, whereafter it was further equilibrated at room temperature for an additional 2 ns.

To reduce the periodicity from 3D to 2D, the coordinates in one of the directions were unwrapped and the boundary conditions in that direction were changed from periodic to shrink-wrapped type. The system was then further equilibrated in the NVT ensemble at room temperature for 1.5 ns. To connect the alumina and polymer layers, we employed a planar indenter to gradually compress the layers over a duration of 4.5 ns, to the degree that the polymer would reach the target density. The planar indenter was then held fixed for an additional 1.5 ns while the system was equilibrated at room temperature, whereafter it was slowly removed (during 1.5 ns) from the surface.

This scheme would result in 2D layered structures such as that depicted in Fig. 1. We considered interfacial samples of two sizes with different dimensions, number of chains, chain length and number of monomers per chain as detailed in Table 1. For each system size and functional group type we generated two samples, i.e. in total 12 samples that were subjected to loading and rigid cleavage deformations. However, in the case that the responses were similar we only present results from one simulation, which is considered representative for the overall outcome.

2.3. Tensile and rigid cleavage simulations

Two types of displacement controlled modelling setups were used: (i) tensile and (ii) rigid cleavage simulations. To effectuate the displacement controlled scheme for the tensile approach, two polymer regions comprising free and prescribed atoms were defined with the respective thicknesses h_2 and h_3, see Fig. 1. The top polymer atoms closer to the free surface than $h_3 = 10$ Å were assigned a translational velocity of $\dot{\delta} = 5 \times 10^{-5}$ Å/fs in the out-of-plane direction, see Fig. 1. Because the alumina substrate is much stiffer than the polymers, we assumed it to be rigid and fixed. The interfacial traction was computed as the force from the freely moving polymer atoms acting on the substrate, normalized by the cross-sectional area $w \times t$.

For the rigid cleavage simulations we used a similar approach as to (i), with the exception that all polymer atoms were assigned the same translational displacement in the out-of-plane direction and no coordinate relaxations were made. This gives the rigid interfacial traction-separation behaviour and enables quantification of the impact of functional groups on the strength, without accounting for the aspect of internal polymer yielding mechanisms. Because the forces acting across the interface are pairwise additive, the contribution from pure PE to the traction was extracted and estimates of the force contribution from individual functional groups were made. To this end we considered the interface as a cohesive zone embedded in a rigid bilayer that underwent brittle failure. The deviating properties induced by the functional groups were then considered to be thermodynamic excess properties [45–48], which through normalization with respect to the number groups at the interface were used to quantify the impact of individual groups. These were then fitted to Rose's universal binding energy relation (UBER) [49],

$$F = C\delta \exp\left(-\frac{\delta}{\delta_c}\right) \tag{2}$$

to describe the excess contribution to the interfacial strength. The parameter δ_c was fitted to reproduce the displacement δ at which the maximum excess force, F_{max}, occured, whereafter C was determined from the relation $C = F_{max}/(\delta_c \exp(-1))$ [50].

Table 1
Data for the considered systems. n_{chains} and n_{mono} represent the number of polymer chains and monomers per chain, whereas $n_{polymer}$ and $n_{substrate}$ indicate the total number of particles in the amorphous polymer and substrate, respectively. The geometrical dimensions w, t and h_2 are defined in Fig. 1 and are given in Å.

System	n_{chains}	n_{mono}	$n_{polymer}$	$n_{substrate}$	w	t	h_2
1	8	90	~4 340	2 520	33.5	33.2	~29
2	20	120	~14 400	5 400	47.9	49.7	~46

2.4. Density functional theory modelling

All DFT simulations in this work were performed using the open-source plane-wave based Quantum Espresso software suite [51,52]. For describing the valence-core interaction we used the ultrasoft pseudopotential approach [53,54] with the valence electron description for C, H, Al and O comprising the $2s^2 2p^2$, $1s^1$, $3s^2 3p^1$ and $2s^2 2p^4$ states, respectively. We chose the kinetic energy cutoff for the plane-wave basis set and k-point density such that the ground state energy was well-converged. To achieve this, we used a kinetic energy cutoff of 60 Ry (1 Ry = 13.6 eV) and the energy cutoff for the electron density set to 600 Ry. We utilized a k-point grid for the first Brillouin zone of the primitive cell for alumina corresponding to a Γ-centered $8 \times 8 \times 3$ grid (for the reciprocal $a \times a \times c$ lattice), generated by means of the Monkhorst–Pack method [55] and a smearing based on the Methfessel-Paxton method with a smearing width corresponding to 0.03 Ry [56]. The resulting lattice parameters of the bulk corundum structure were found to be $a =$ 4.79 and $c = 13.05$ Å, which compare well with experimental data of 4.75 and 12.97 Å [57], respectively. For the slab calculations we utilized a 12 layer 2×1 hexagonal supercell with a vacuum interface between periodic images no less than 12 Å thick and a dipole correction to cancel the electrostatic interaction [58]. The adopted k-point mesh was made commensurate with the bulk alumina phase.

Owing to the importance of vdW interaction in the considered system, we adopted an exchange–correlation functional based on the vdW-DF method, specifically the recent consistent-exchange vdW-DF-cx version [59,60]. Such non-local functionals have shown an improved ability to capture many of the characteristics of crystalline polymers and organic molecules that local or semi-local formulations, such as conventional local density or generalized gradient approximations, fail to reproduce e.g. binding strength, intermolecular interaction, lattice parameter and elastic properties [27,61,9], some of which are highly relevant for the present study.

3. Results and discussion

3.1. Molecular adsorption onto (0001)-surface

To benchmark the performance of the utilized potential in terms of bonding of functional groups onto alumina surfaces, we investigate how the potential energy varies for ethanol and acetaldehyde molecules at different distances from the surface by means of DFT. For the case of ethanol we consider the non-dissociated ground state configuration found in previous DFT works [9,10], which is a slightly tilted horizontal configuration where the hydroxyl O adheres to the top Al site as depicted in Fig. 2(a). For the acetaldehyde adsorption we consider two different configurations that we refer to horizontal and vertical configurations from which the coordinates are relaxed, see Fig. 2(b) and (c), respectively.

For ethanol, the binding energy and equilibrium Al-O bond length between the substrate and molecule correspond to 1.65 eV and 1.91 Å, respectively, see Fig. 2(a), which concur with those of previous DFT works [9,10]. For acetaldehyde, the ground state is the horizontal configuration depicted in Fig. 2(b), which has an adhesion energy and Al-O bond length of 1.79 eV and 1.90 Å, respectively, see Fig. 2(b). This configuration is found to be more stable than the vertical configuration, for which the adhesion energy and Al-O bond length correspond to 1.57 eV and 1.91 Å, respectively, see Fig. 2(c).

The sixth power mixing rule is the starting point for the mixed potential between the Al and molecular O. For the case of hydroxyl O, this approach gives a good representation of the binding energy, which is 1.66 eV, see Fig. 2(a). Despite that the bond length is substantially underestimated compared to DFT predictions to about 1.45 Å, we opted not to alter the potential parameters since the binding energy is the important factor that dictates the binding strength to the substrate. The opposite trend is observed for acetaldehyde molecule adsorption; the equilibrium bond length of 1.89 Å is in good agreement with DFT data, whereas the binding energy of 0.69 eV is much too low and would lead to underestimated bond strength. To improve the binding energy we adjusted the LJ-9–6 parameters of (1) for the Al and carbonyl O pair to $\varepsilon = 0.048$ kcal/mol and $\sigma = 2.45$ Å, which increases the binding energy to 1.90 and 1.70 eV for the horizontal and vertical configurations, respectively, that are in acceptable agreement with the DFT data, see Fig. 2(b) and (c). This adjustment is made at the expense of the equilibrium bond length, which is reduced to about 1.45 Å for both configurations.

3.2. Tensile simulations

Before turning the attention towards functionalized PE, we study the traction-separation behaviour of the PE-alumina system without any functional groups present. The results indicate that the traction-separation curves and deformation behaviours for such systems are similar for both sizes, with the exception that the smaller system ruptures at a lower displacement, see Fig. 3. This is due to the fact that the size of the polymer region dictates the amount of mechanical work that the material can sustain before fracture.

During the initial stages the polymer undergoes a rather uniform deformation, which manifests in a substantial increase in traction until the peak stress (∼100 MPa) is reached. This is followed by a significant reduction in stress that coincides with the formation of fibrils consisting of polymer chains aligned in the tensile direction, see Fig. 3(c) and (d). The entangled parts of the fibril chains in the proximity of the substrate exert tensile forces on the interacting chains, which gives rise to a non-zero traction at the polymer/substrate interface. Increasing the strain further leads to gradual thinning of fibrils, increased disentanglement in the amorphous region at the substrate and chain detachment from the substrate, which gradually reduce the traction until rupture occurs. Similar polymer yielding behaviour has been found previously for semi-crystalline PE [62,28], where the crystalline parts remain rigid and free from plastic deformation, while the decreasing amorphous parts feed the gradually thinning fibrils. These results imply that the traction, and consequently work of fracture (related to the area under the traction-separation curve), is a result of three mechanisms; (i) the resistance to chain slip of the fibrils, (ii) resistance to fibril chain disentanglement and (iii) polymer chain detachment from the substrate, which jointly dictate the tensile force that can be transmitted from the upper part, via the fibrils, to the substrate during the separation.

For most specimens it was found that polymer residues consisting of individual polymer chains adhered to the alumina surface following failure, suggesting that a clean fracture at the interface between the polymer and substrate rarely occurred. This behaviour is in line with that found for the interface between Cu and PVDF [21]. We note that it deviates from that found for atomistic tensile modelling of pyrophillite-PVA interfaces [16], where no remaining polymer residues were observed on the substrate and the polymer only underwent small deformations ($\delta \sim 10$ Å as opposed to $\delta > 100$ Å for PE) before a clean separation between the layers was obtained. These seemingly disparate behaviours are believed to be related to the generally higher stiffness of PVA and its high glass transition temperature (∼ 80°C) compared to PE

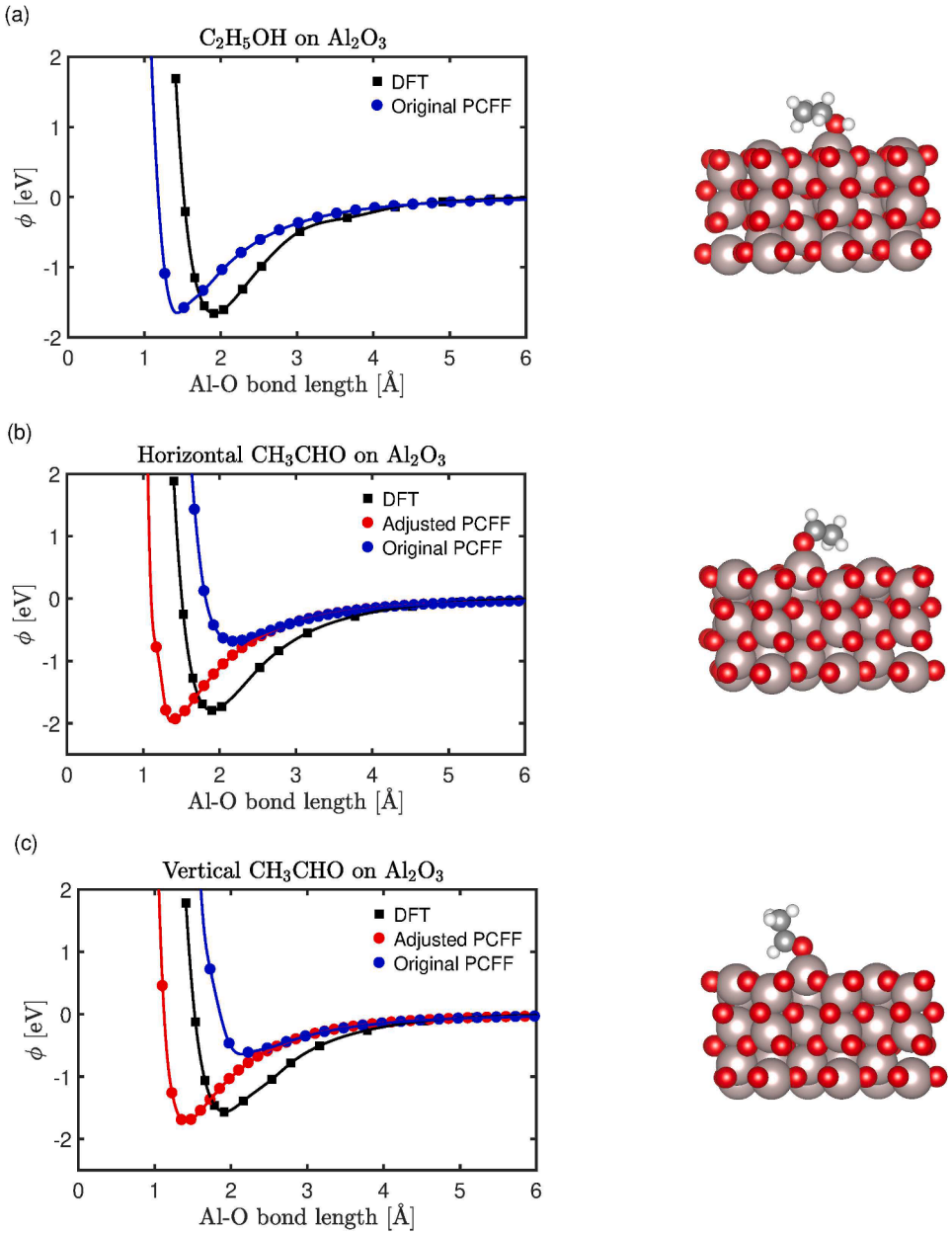

Fig. 2. Adhesion energy for (a) ethanol, (b) horizontal and (c) vertical acetaldehyde on α-alumina (0001)-surface. The left panel displays the energy vs. displacement and the right panel indicates the ground state configuration.

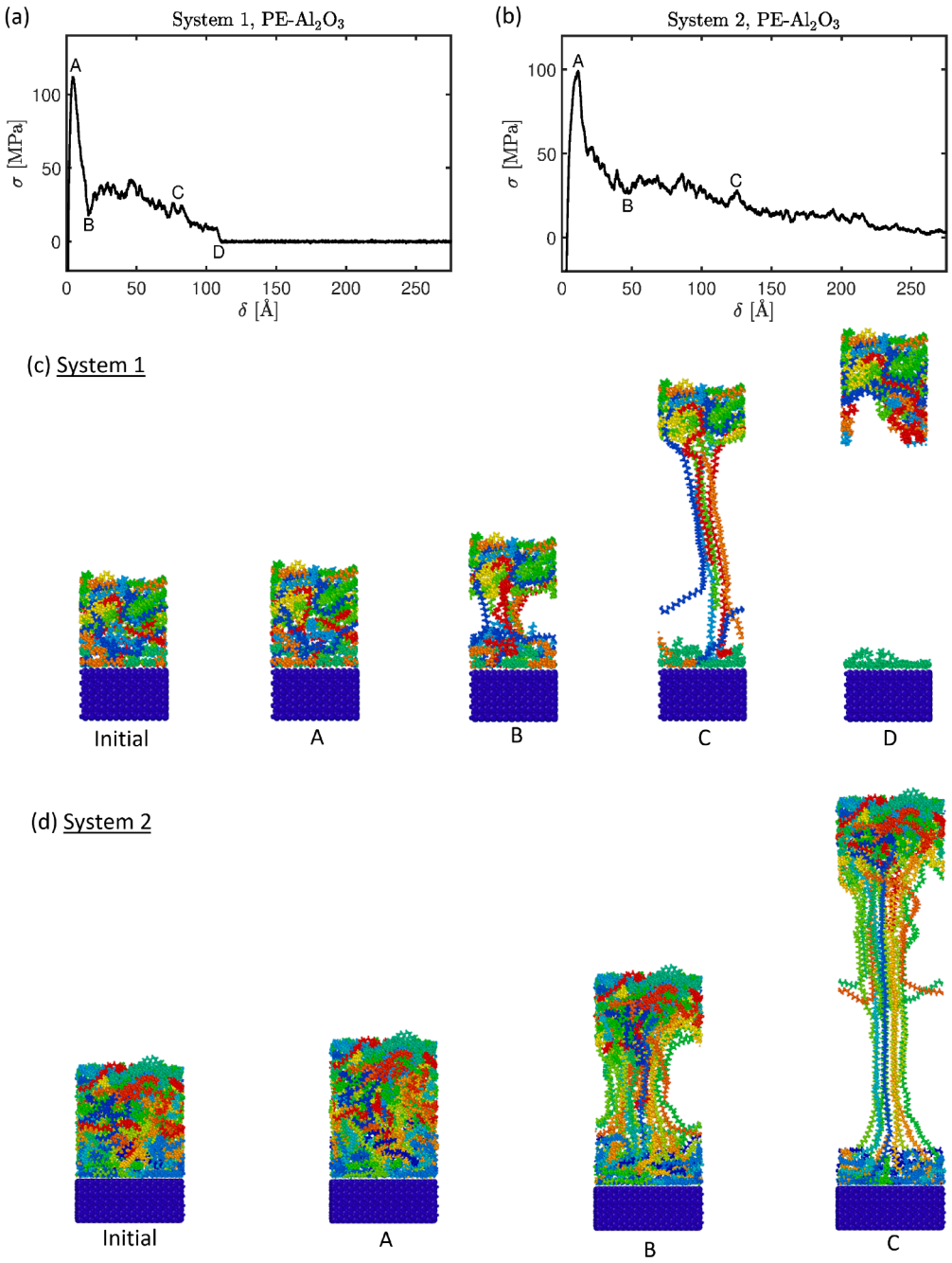

Fig. 3. Traction-separation curves for the PE-alumina interface of (a) system 1 and (b) system 2. (c) and (d) represent sequential configuration snapshots corresponding to the events A-D in the respective traction-separation curve. The polymer chains in (c) and (d) are coloured based on molecular ID.

and PVDF ($\sim -35 - -20°C$).

As demonstrated by Figs. 4 and 5, the introduction of functional groups gives rise to more or less the same deformation behaviour observed in Fig. 2(c) and (d). Moreover, the initial traction-separation behaviour is found to resemble those for the systems without functional groups. However, as indicated in Fig. 4(a) and (b) as well as Fig. 5 (a) and (b), for most cases spikes in the traction-separation curves emerge following fibril initialization and lead to increased traction. Such events are found to coincide with the detachment of the functional groups from top Al sites at the substrate, as indicated by Fig. 4(c) and (d). The shapes of most spikes are similar, but for some, which are found to be either higher, wider or both, there is more than one functional group detaching within a short time interval, see Fig. 5(c).

In Fig. 4(b) we provide a direct comparison between two equivalent systems containing the same concentration of carbonyl groups, but only one of them undergoes functional group detachment from the substrate. It is seen that without detachments the traction-separation curve bears strong resemblance with that in Fig. 3(b), suggesting that the functional groups do not have a substantial impact on the chain slip or disentanglement. Moreover, the initial peak stress of the traction-separation curves does not to increase following the introduction of the functional groups in the polymer. This confirms that the notable increase in work of fracture emanate from their detachment from the substrate.

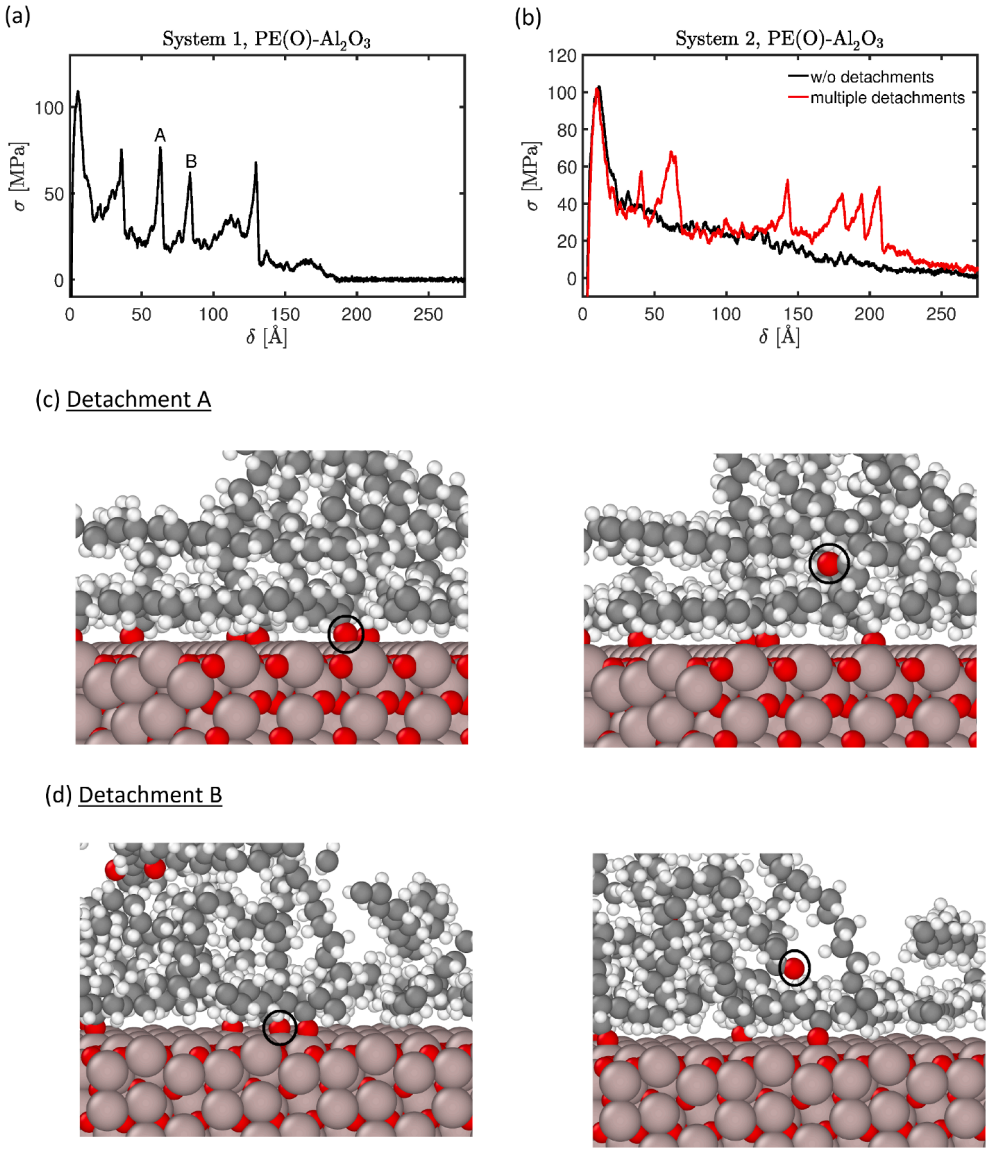

Fig. 4. Traction-separation curves for the PE(O)-alumina interface of (a) system 1 and (b) system 2. Carbonyl detachments from the substrate indicated by the peaks A and B in (a) are depicted in (c) and (d), respectively.

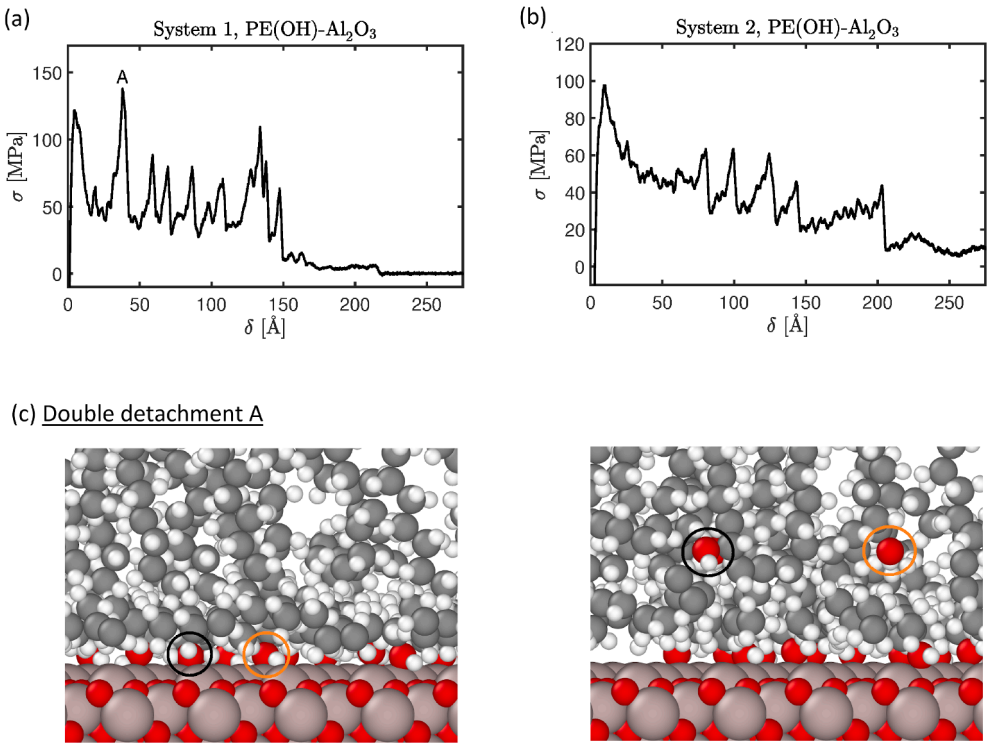

Fig. 5. Traction-separation curves for the PE(OH)-alumina interface of (a) system 1 and (b) system 2. (c) Double hydroxyl detachment from the substrate indicated by the peak A in (a).

3.3. Cleavage simulations

In Fig. 6 we present the excess force for individual carbonyl and hydroxyl groups. It is seen that there is only a minor variation in terms of peak force and inflection point among the different system sizes, indicating that the excess contribution to the traction indeed can be described by the UBER ansatz in (2). The respective fitted values of C and δ_c correspond to 7.2 nN/Å and 0.40 Å for carbonyl and 8.9 nN/Å and 0.33 Å for hydroxyl, leading to a maximum value of about 1.1 nN for the excess force of both functional group types. In accordance with the DFT data in Fig. 2, this is an indication that both functional types give rise to similar binding energies and detachment behaviours. By translating the maximum force magnitudes to traction for the considered systems they become of the order of 95 and 50 MPa per functional group for the large and small sample types, respectively. These results agree with the observed spikes in Fig. 4(a)-(b) and 5(b) and concur with our previous observation that the functional groups have no notable effect on the deformation and initial traction-separation behaviour, but mainly impacts the post-fibril traction-separation behaviour where the discrete detachments contribute to increased work of separation.

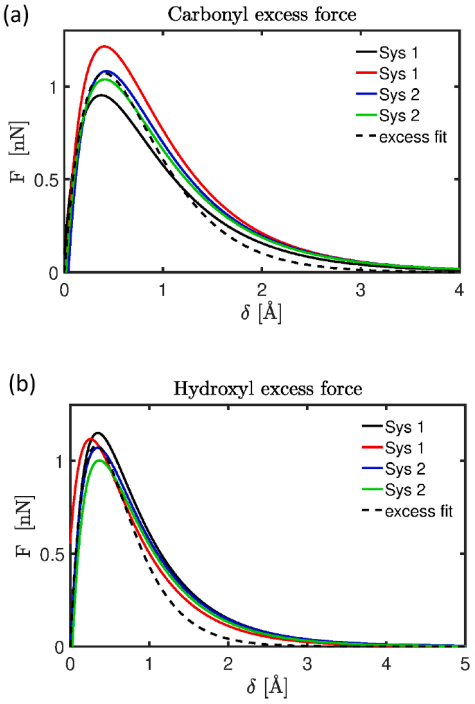

Fig. 6. Computed and fitted excess forces for individual (a) carbonyl groups and (b) hydroxyl groups for rigid separation.

4. Summary and conclusions

In the present work we have used quantum mechanical DFT and classical atomistic modelling to investigate the impact of functional groups on the interfacial adhesion and deformation behaviour between alumina and ozone treated PE containing carbonyl and hydroxyl groups. It is found that both group types adsorb at the top Al-sites on the alumina surface and give rise to a bonding energy of the order of 1.7 eV and a threshold excess force of about 1.1 nN per functional unit, which confirm improved adhesion onto the substrate.

The overall deformation behaviour is ductile in character with localized deformations in the polymer region consisting of chain detachments, slip and disentanglement, as expected for PE, which has a low glass temperature. This behaviour is similar to that of semi-crystalline PE, where the amorphous parts initially undergo substantial deformation, while the crystalline parts are almost free from deformation. When doped with functional groups the deformation behaviour does not change notably, but we observe localized increases

in traction which are found to coincide with the detachment of single or multiple functional groups from the substrate. This suggests that the functional groups do not increase the resistance to chain slip or disentanglement, but improve the resistance to substrate detachment, which manifests in discrete spikes in the traction-separation curves that lead to increased work of fracture.

Author contributions

The manuscript is written through contributions of all authors. All authors have given approval to the final version of the manuscript and declare no competing interest.

Data availability

The data required to reproduce these findings are available from the corresponding author upon reasonable request.

CRediT authorship contribution statement

Pär A.T. Olsson: Conceptualization, Methodology, Investigation, Formal analysis, Writing - original draft. **Erik Bergvall:** Conceptualization, Writing - review & editing.

Declaration of Competing Interest

The authors declare that they have no known competing financial interests or personal relationships that could have appeared to influence the work reported in this paper.

Acknowledgements

The authors gratefully thank the Swedish Foundation for Strategic Research (grant SM17-0020), the Crafoord foundation (grant 20160740) and Tetra Pak Packaging Solutions AB for providing the financial means to make this project possible. The authors acknowledge Dr. Barbara M. Poliks at Binghamton University, NY, for helpful discussions and the Swedish National Infrastructure for Computing (SNIC) at the National Supercomputer Centre (NSC), Linköping University and at the High Performance Computing Center North (HPC2N), Umeå University, for providing the computational resources needed to conduct this study. Parts of the virtual sample generations in the present work were done using the MedeA software version 3.0 [34].

References

[1] J.D. Spikes, Photodegradation of Foods and Beverages, Springer, US, Boston, MA, 1981, pp. 39–85.
[2] M. Bekbölet, Light effects on food, J. Food Prot. 53 (5) (1990) 430–440.
[3] B. Lu, Y. Zhao, Photooxidation of phytochemicals in food and control: a review, Ann. N. Y. Acad. Sci. 1398 (1) (2017) 72–82.
[4] E. Andreasson, Mechanics and failure in thin material layers - towards realistic package opening simulations, Ph.D. Thesis (2019) Blekinge Institute of Technology.
[5] D. Hegemann, H. Brunner, C. Oehr, Plasma treatment of polymers for surface and adhesion improvement, Nucl. Instrum. Methods Phys. Res., Sect. B 208 (2003) 281–286.
[6] J. Yamauchi, A. Yamaoka, K. Ikemoto, T. Matsui, Reaction mechanism for ozone oxidation of polyethylene as studied by ESR and IR spectroscopies, Bull. Chem. Soc. Jpn. 64 (4) (1991) 1173–1177.
[7] H. Metiu, S. Chretien, Z. Hu, B. Li, X. Sun, Chemistry of Lewis acid-base pairs on oxide surfaces, J. Phys. Chem. C 116 (19) (2012) 10439–10450.
[8] J. van den Brand, P.C. Snijders, W.G. Sloof, H. Terryn, J.H.W. de Wit, Acid-base characterization of aluminum oxide surfaces with XPS, J. Phys. Chem. B 108 (19) (2004) 6017–6024.
[9] K. Johnston, A van der Waals density functional study of the adsorption of ethanol on the α-alumina (0001) surface, Surf. Sci. 621 (2014) 16–22.
[10] H.-N. Chiang, S. Nachimuthu, Y.-C. Cheng, N.P. Damayanti, J.-C. Jiang, A DFT study of ethanol adsorption and decomposition on α-Al_2O_3(0001) surface, Appl. Surf. Sci. 363 (2016) 636–643.
[11] T. Semoto, Y. Tsuji, K. Yoshizawa, Molecular understanding of the adhesive force between a metal oxide surface and an epoxy resin, J. Phys. Chem. C 115 (23) (2011) 11701–11708.
[12] Ø. Borck, P. Hyldgaard, E. Schröder, Adsorption of methylamine on α-Al_2O_3 and α-Cr_2O_3-(0001): Density functional theory, Phys. Rev. B 75 (2007), 035403.
[13] J. Blomqvist, P. Salo, Adsorption of benzene, phenol, propane and carbonic acid molecules on oxidized al(111) and α-Al_2O_3(0001) surfaces: a first-principles study, J. Phys.: Condens. Matter 21 (22) (2009), 225001 .
[14] J. Blomqvist, P. Salo, First-principles study for the adsorption of segments of BPA-PC on α-Al_2O_3(0001), Phys. Rev. B 84 (2011), 153410 .
[15] C.-Y. Cheng, K.-J. Lee, Y. Li, B.-C. Wang, Molecular dynamics simulation of polymers adsorbed onto an alumina surface, J. Adhes. Sci. Technol. 12 (7) (1998) 695–712.
[16] B. Paliwal, W.B. Lawrimore, M.Q. Chandler, M.F. Horstemeyer, Nanomechanical modeling of interfaces of polyvinyl alcohol (PVA)/clay nanocomposite, Phil. Mag. 97 (15) (2017) 1179–1208.
[17] G. Xu, H. Wang, Molecular dynamics study of interfacial mechanical behavior between asphalt binder and mineral aggregate, Constr. Build. Mater. 121 (2016) 246–254.
[18] G. Xu, H. Wang, Study of cohesion and adhesion properties of asphalt concrete with molecular dynamics simulation, Comput. Mater. Sci. 112 (2016) 161–169.
[19] S. Yang, F. Gao, J. Qu, A molecular dynamics study of tensile strength between a highly-crosslinked epoxy molding compound and a copper substrate, Polymer 54 (18) (2013) 5064–5074.
[20] S. Yang, J. Qu, An investigation of the tensile deformation and failure of an epoxy/cu interface using coarse-grained molecular dynamics simulations, Modelling Simul. Mater. Sci. 22 (6) (2014), 065011 .
[21] S. Lee, Molecular dynamics study of the separation behavior at the interface between PVDF binder and copper current collector, J. Nanomater. 2016 (2016) 4253986.
[22] J. Wu, S. Nagao, Z. Zhang, J. He, Deformation and fracture of nano-sized metal-coated polymer particles: A molecular dynamics study, Eng. Fract. Mech. 150 (2015) 209–221.
[23] J. Yang, C. Weng, J. Lai, T. Ding, H. Wang, Molecular dynamics simulation on the influences of nanostructure shape, interfacial adhesion energy, and mold insert material on the demolding process of micro-injection molding, Polymers 11 (10) (2019) 1573.
[24] C. Weng, J. Yang, D. Yang, B. Jiang, Molecular dynamics study on the deformation behaviors of nanostructures in the demolding process of micro-injection molding, Polymers 11 (3) (2019) 470.
[25] C. Weng, D. Yang, M. Zhou, Molecular dynamics simulations on the demolding process for nanostructures with different aspect ratios in injection molding, Micromachines 10 (10) (2019) 636.
[26] S. Plimpton, Fast parallel algorithms for short-range molecular dynamics, J. Comput. Phys. 117 (1) (1995) 1–19.
[27] P.A.T. Olsson, E. Schröder, P. Hyldgaard, M. Kroon, E. Andreasson, E. Bergvall, Ab initio and classical atomistic modelling of structure and defects in crystalline orthorhombic polyethylene: Twin boundaries, slip interfaces, and nature of barriers, Polymer 121 (2017) 234–246.
[28] P.A.T. Olsson, P.J. in 't Veld, E. Andreasson, E. Bergvall, E. Persson Jutemar, V. Petersson, G.C. Rutledge, M. Kroon, All-atomic and coarse-grained molecular dynamics investigation of deformation in semi-crystalline lamellar polyethylene, Polymer 153 (2018) 305 – 316.
[29] H. Sun, Compass: An ab initio force-field optimized for condensed-phase applications-overview with details on alkane and benzene compounds, J. Phys. Chem. B 102 (38) (1998) 7338–7364.
[30] H. Sun, Force field for computation of conformational energies, structures, and vibrational frequencies of aromatic polyesters, J. Comput. Chem. 15 (7) (1994) 752–768.
[31] H. Sun, Ab initio calculations and force field development for computer simulation of polysilanes, Macromolecules 28 (3) (1995) 701–712.
[32] W.L. Jorgensen, J. Tirado-Rives, The OPLS [optimized potentials for liquid simulations] potential functions for proteins, energy minimizations for crystals of cyclic peptides and crambin, J. American Chem. Soc. 110 (6) (1988) 1657–1666.
[33] W.L. Jorgensen, D.S. Maxwell, J. Tirado-Rives, Development and testing of the OPLS all-atom force field on conformational energetics and properties of organic liquids, J. American Chem. Soc. 118 (45) (1996) 11225–11236.
[34] MedeA ® 3.0 (Materials Exploration and Design Analysis), Materials Design Inc., Angel Fire, NM, USA, 2019.
[35] L. Zhao, L. Liu, H. Sun, Semi-ionic model for metal oxides and their interfaces with organic molecules, J. Phys. Chem. C 111 (28) (2007) 10610–10617.
[36] A. Stukowski, Visualization and analysis of atomistic simulation data with OVITO–the open visualization tool, Modelling Simul. Mater. Sci. Eng.18 (1) 015012.
[37] X.-G. Wang, A. Chaka, M. Scheffler, Effect of the environment on α-Al_2O_3(0001) surface structures, Phys. Rev. Lett. 84 (2000) 3650–3653.
[38] Z. Lodziana, J.K. Nørskov, P. Stoltze, The stability of the hydroxylated (0001) surface of α-Al_2O_3, J. Chem. Phys. 118 (24) (2003) 11179–11188.
[39] P.J. Eng, T.P. Trainor, G.E. Brown, G.A. Waychunas, M. Newville, S.R. Sutton, M. L. Rivers, Structure of the hydrated α-Al_2O_3 (0001) surface, Science 288 (5468) (2000) 1029–1033.
[40] P. Thissen, G. Grundmeier, S. Wippermann, W.G. Schmidt, Water adsorption on the α-Al_2O_3(0001) surface, Phys. Rev. B 80 (2009), 245403 .
[41] Ø. Borck, E. Schröder, First-principles study of the adsorption of methanol at the α-Al_2O_3(0001) surface, J. Phys.: Condens. Matter 18 (1) (2006) 1–12.

[42] T.J. Godin, J.P. LaFemina, Atomic and electronic structure of the corundum α-alumina (0001) surface, Phys. Rev. B 49 (1994) 7691–7696.
[43] S. Nosé, A unified formulation of the constant temperature molecular dynamics methods, J. Chem. Phys. 81 (1) (1984) 511–519.
[44] W.G. Hoover, Canonical dynamics: equilibrium phase-space distributions, Phys. Rev. A 31 (1985) 1695–1697.
[45] A. Van der Ven, G. Ceder, The thermodynamics of decohesion, Acta Mater. 52 (5) (2004) 1223–1235.
[46] R.A. Enrique, A. Van der Ven, Solute embrittlement of SiC, J. Appl. Phys. 116 (11) (2014), 113504 .
[47] R.A. Enrique, A. Van der Ven, Decohesion models informed by first-principles calculations: The ab initio tensile test, J. Mech. Phys. Solids 107 (2017) 494–508.
[48] P.A.T. Olsson, J. Blomqvist, Intergranular fracture of tungsten containing phosphorus impurities: A first principles investigation, Comput. Mater. Sci. 139 (2017) 368–378.
[49] J.H. Rose, J. Ferrante, J.R. Smith, Universal binding energy curves for metals and bimetallic interfaces, Phys. Rev. Lett. 47 (1981) 675–678.
[50] P.A.T. Olsson, K. Kese, M. Kroon, A.-M. Alvarez Holston, Ab initio-based fracture toughness estimates and transgranular traction-separation modelling of zirconium hydrides, Modell. Simul. Mater. Sci. Eng. 23 (4) (2015) 045015.
[51] P. Giannozzi, S. Baroni, N. Bonini, M. Calandra, R. Car, C. Cavazzoni, D. Ceresoli, G.L. Chiarotti, M. Cococcioni, I. Dabo, A. Dal Corso, S. de Gironcoli, S. Fabris, G. Fratesi, R. Gebauer, U. Gerstmann, C. Gougoussis, A. Kokalj, M. Lazzeri, L. Martin-Samos, N. Marzari, F. Mauri, R. Mazzarello, S. Paolini, A. Pasquarello, L. Paulatto, C. Sbraccia, S. Scandolo, G. Sclauzero, A.P. Seitsonen, A. Smogunov, P. Umari, R. M. Wentzcovitch, Quantum espresso: a modular and open-source software project for quantum simulations of materials, J. Phys.: Condens. Matter 21 (39) (2009) 395502 (19pp).
[52] P. Giannozzi, O. Andreussi, T. Brumme, O. Bunau, M. Buongiorno Nardelli, M. Calandra, R. Car, C. Cavazzoni, D. Ceresoli, M. Cococcioni, N. Colonna, I. Carnimeo, A.D. Corso, S. de Gironcoli, P. Delugas, R.A.D. Jr, A. Ferretti, A. Floris, G. Fratesi, G. Fugallo, R. Gebauer, U. Gerstmann, F. Giustino, T. Gorni, J. Jia, M. Kawamura, H.-Y. Ko, A. Kokalj, E. Kücükbenli, M. Lazzeri, M. Marsili, N. Marzari, F. Mauri, N.L. Nguyen, H.-V. Nguyen, A. Otero-de-la-Roza, L. Paulatto, S. Ponce, D. Rocca, R. Sabatini, B. Santra, M. Schlipf, A.P. Seitsonen, A. Smogunov, I. Timrov, T. Thonhauser, P. Umari, N. Vast, X. Wu, S. Baroni, Advanced capabilities for materials modelling with quantum espresso, J. Phys.: Condens. Matter 29 (46) (2017), 465901 .
[53] D. Vanderbilt, Soft self-consistent pseudopotentials in a generalized eigenvalue formalism, Phys. Rev. B 41 (1990) 7892–7895.
[54] K.F. Garrity, J.W. Bennett, K.M. Rabe, D. Vanderbilt, Pseudopotentials for high-throughput DFT calculations, Comput. Mater. Sci. 81 (2014) 446–452.
[55] H.J. Monkhorst, J.D. Pack, Special points for brillouin-zone integrations, Phys. Rev. B 13 (1976) 5188–5192.
[56] M. Methfessel, A.T. Paxton, High-precision sampling for brillouin-zone integration in metals, Phys. Rev. B 40 (1989) 3616–3621.
[57] I. Levin, D. Brandon, Metastable alumina polymorphs: Crystal structures and transition sequences, J. Am. Ceram. Soc. 81 (8) (1998) 1995–2012.
[58] L. Bengtsson, Dipole correction for surface supercell calculations, Phys. Rev. B 59 (1999) 12301–12304.
[59] K. Berland, P. Hyldgaard, Exchange functional that tests the robustness of the plasmon description of the van der Waals density functional, Phys. Rev. B 89 (2014), 035412 .
[60] K. Berland, C.A. Arter, V.R. Cooper, K. Lee, B.I. Lundqvist, E. Schröder, T. Thonhauser, P. Hyldgaard, van der Waals density functionals built upon the electron-gas tradition: Facing the challenge of competing interactions, J. Chem. Phys. 140 (18) (2014) 18A539.
[61] P.A.T. Olsson, P. Hyldgaard, E. Schröder, E. Persson Jutemar, E. Andreasson, M. Kroon, Ab initio investigation of monoclinic phase stability and martensitic transformation in crystalline polyethylene, Phys. Rev. Materials 2 (2018), 075602 .
[62] I.-C. Yeh, J.W. Andzelm, G.C. Rutledge, Mechanical and structural characterization of semicrystalline polyethylene under tensile deformation by molecular dynamics simulations, Macromol. 48 (12) (2015) 4228–4239.